# 4

# Numerical study of three-dimensional instabilities of Czochralski melt flow driven by buoyancy convection, thermocapillarity and rotation

**A. Yu. Gelfgat**
School of Mechanical Engineering, Faculty of Engineering, Tel-Aviv University
Ramat Aviv 69978, Tel-Aviv, Israel

## Abstract

*A recent numerical approach for the study of three-dimensional instabilities of axisymmetric melt flows in Czochralski crucible is described. The convergence studies and comparisons with previously published experimental and numerical data are reported. Convergence requirements are estimated. Basing on a certain experimental configuration we give an example of the stability diagram which shows how the critical temperature difference varies with the*

Correspondence/Reprint request: Prof. A. Yu. Gelfgat, School of Mechanical Engineering, Faculty of Engineering, Tel-Aviv University, Ramat Aviv 69978, Tel-Aviv, Israel. E-mail: gelfgat@eng.tau.ac.il

*crystal rotation. We show also that the critical temperature difference can be significantly increased by a weak rotation of the crucible and report the corresponding stability diagrams.*

# 1. Introduction

Since the early works of D.T.J Hurle [1-3] it was argued that formation of defects and inhomogeneities in the bulk crystals grown from melt is caused by instabilities of melt flow. The early evidence of connection between the melt flow instabilities and crystal defects was reported in [1-6]. Nowadays this connection became a common knowledge (see, e.g., [7-12]). The melt flow and its instabilities are driven by the buoyancy forces, by thermocapillary and concentration-capillary forces caused by the dependence of surface tension on temperature and concentration, and by rotation of crystal and possibly of other parts of a bulk crystal growth setup. Since melt flows are always bounded by crucible walls, capillary surfaces and the crystal itself, their instabilities usually differ qualitatively from the instabilities in infinite domains, e.g., infinite convective layers, unbounded shear flows or Taylor-Couette configuration. The recognition of this fact motivated a large number of works that studied stability of simplified model flows in confined domains. These studies, which are reviewed in [13-15], considered, as a rule, the action of only one of flow driving mechanisms. Nevertheless, they lead to the understanding of many important facts, such as an existence of multiple steady and unsteady states and non-monotonic, non-trivial behavior of flow stability properties. At the same time these studies did not yield a quantitative measure of instability in practically important crystal growth processes, where the whole process and the melt flow in particular are much more complicated.

In this paper we describe a possible way to arrive to some quantitative results on stability of melt flow taking into account all possible driving mechanisms. We focus on melt flow in a model of Czochralski crystal growth setup. The choice of the Czochralski setup is motivated by its most intensive use in the manufacturing of bulk monocrystal [16,17], as well as by its relative complexity with respect to other bulk crystal growth techniques, e.g., floating zone and Bridgman growth. The description of the Czochralski crystal growth technique can be found in [18]. Within the Czochralski model considered here we incorporate the combined action of the buoyancy, thermocapillary, centrifugal and Coriolis forces, and allow for an arbitrary heating of the crucible walls and bottom and for an arbitrary cooling of the melt interface. In this paper we shortly review the experimental evidence of different instabilities in the Czochralski melt flow and the corresponding model experimental studies. We discuss also existing computational approaches being used to model and study these instabilities numerically. Then we describe some recent

achievements of our research group in the developing of numerical approach to three-dimensional stability analysis of Czochralski melt flow, describe some recent results and define the target problems for possible future research.

Experimental studies of instabilities in the Czochralski melt flow can be carried out either by measuring the temperature [19-40], or velocity [38] oscillations at some fixed points into the melt or by visualization of the melt flow either on its free surface [34,41-48], or inside the container using transparent liquid and crucible for a model experiment [30,33,51,52]. When the melt is not transparent the visualization data can be achieved by X-ray radiography [53-62] or by arrays of thermocouples [63,64] and conductive anemometer probes [64]. Most of the cited works studied the supercritical regimes of melt flow and did not focus on the question under which conditions the axisymmetric steady flow turns into three-dimensional or oscillatory. Attempts to study this transition and to measure the critical values of parameters were made in [19,31-33] and other studies. Unfortunately, in most of such studies the thermal boundary conditions are not definite enough to reproduce them in a computational code. For example, our attempts to reproduce results of [32] failed because we were not able to fit thermal boundary condition at the melt surface to conditions of the experiment.

Early numerical studies of instabilities, as well as some of the recent ones, consider transition from steady to oscillatory flow regimes in the axisymmetric flow configurations [28,65-75]. All these studies did not account for possible three-dimensional instabilities and therefore did not yield the complete answers on the stability limits and possible flow transitions. Besides that all these studies are performed on rather coarse grids with less than 100 nodes in one spatial direction, which is rather unexpected for the studies that appeared during last years. The necessary grid resolution will be discussed below. Since most of experimental flow visualizations observe three-dimensional flow patterns the comprehensive numerical analysis should be three-dimensional, which is really the case for most of numerical studies [76-120]. The numerical studies are even more restricted to a coarse grid resolution, however some of them, e.g., [107], approach an order of 100 nodes in each spatial direction.

Obviously, accurate fully three-dimensional computations do provide feasible results, however they are extremely CPU-time consuming even when the most powerful computers are used. In many cases computer restrictions do not allow one to perform three-dimensional computations to within the numerical accuracy needed for correct resolution of all kinds of possible flow perturbations. These restrictions can be partially removed in cases when the primary instabilities of initially axisymmetric flows are studied. A big part of bulk crystal growth setups including the Czochralski setup are built to support axisymmetric conditions and considerable efforts are applied to keep the axisymmetric states stable. This leads to a problem of accurate computation of

a primary instability of an axisymmetric steady state of a process. Possible instabilities must be studied as functions of governing parameters of the process to enable search for most stable conditions and possible means of stability control. From a formal mathematical view point this problem needs a calculation of an axisymmetric steady state of a process followed by the computation of the spectrum of the governing equations linearized in the vicinity of the steady state. To be realized numerically this approach needs a fast solver for calculation of steady state base flows and an effective eigensolver to approach the linear stability problem. This task seemed impossible for many years and started to be attacked only recently [121-124].

The stability solver of this king is being developed in our laboratory. It has been validated via a series of benchmark problems [125-127] and is being applied now to a model corresponding to the melt flow in Czochralski crucible. In the following we describe our numerical approach and some test calculations that allow us to validate the code and to study the convergence of critical parameters with mesh refinement. Then we report several examples of parametric stability studies based on the configuration of recently published experimental study [35]. It is emphasized that according to our recent understanding of instabilities observed in simpler model flows (see [13-15] and references therein) the flow stability strongly depends on fluid properties and geometry of the flow region. Therefore, an attempt to study of stability of melt flow in the Czochralski configuration for a general case would be meaningless since it is not possible to account for all possible variations of the setup and different physical properties of materials. To perform a meaningful study we always need to connect our numerical model to some published experimental configuration. A successful comparison with an experiment, as it is done below for the experiment of [19], yields a necessary validation of the recent code, which is essential for its further development and extension.

## 2. Formulation of the problem

The model of the Czochralski melt flow is sketched in Fig.1. The flow is located in a cylindrical crucible, which can be heated or cooled arbitrarily by posing a constant temperature, constant heat flux, convective cooling or radiative heating/cooling conditions at its bottom and sidewall. The bottom and the sidewall are no-slip. The crystal is modeled by a no-slip isothermal surface. The crystal and the crucible can rotate around their common axis in any direction with independent angular velocities. The melt surface located between the crucible wall and the crystal is assumed to be flat and subjected to the action of the thermocapillary force. It can be cooled by external convection or by radiation. Clearly, this is a simplified model, which does not account for many important phenomena, however allows us to study the main features of
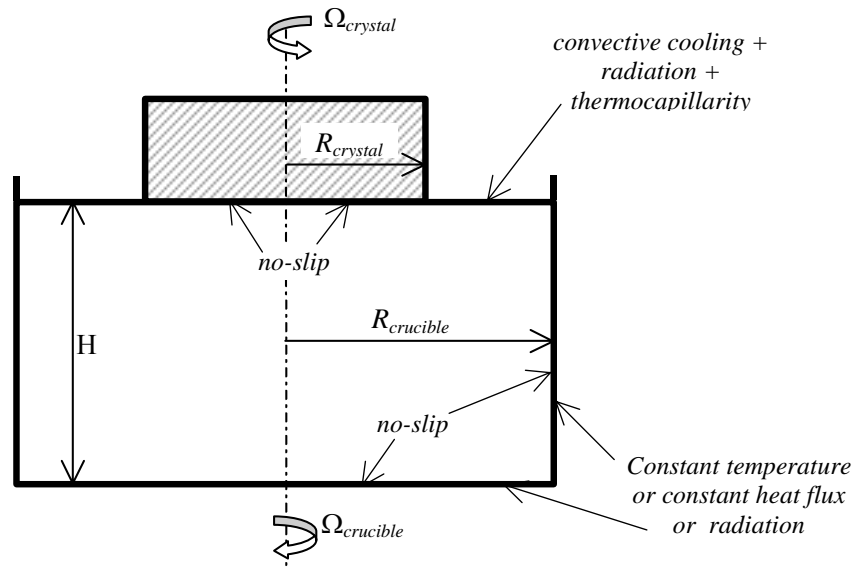
**Figure 1.** Sketch of the model problem.

the instability of melt flow driven by buoyancy convection, thermocapillary convection and rotation. In particular, the considered model corresponds to the experimental configurations of [31-33,35,36].

The problem is formulated for a Boussinesq fluid with kinematic viscosity $\nu$, density $\rho$ and thermal diffusivity $\chi$ in the region $0 \le r \le R_{crucible}$, $0 \le z \le H$. The flow is described by the momentum, continuity and energy equations in cylindrical coordinates. To render the equations dimensionless we use the scales $R_{crucible}$, $R_{crucible}^2/\nu$, $\nu/R_{crucible}$, $\rho(\nu R_{crucible})^2$ for length, time, velocity and pressure respectively. The temperature is rendered dimensionless by the relation $T = (T^* - T_{cold}^*)/(T_{hot}^* - T_{cold}^*)$, where $T_{hot}^*$ and $T_{cold}^*$ are the maximal and minimal temperatures at the boundaries of the flow region. The set of Boussinesq equations for the non-dimensional velocity $\mathbf{v} = \{v_r, v_\theta, v_z\}$, temperature $T$ and pressure $p$ in the domain $0 \le r \le 1, 0 \le z \le A$ reads

$$\frac{\partial \mathbf{v}}{\partial t} + (\mathbf{v} \cdot \nabla)\mathbf{v} = -\nabla p + \Delta \mathbf{v} + Gr\,\theta\,\mathbf{e}_z \tag{1}$$

$$\frac{\partial T}{\partial t} + (\mathbf{v} \cdot \nabla)T = \frac{1}{Pr}\Delta T \quad, \qquad \nabla \cdot \mathbf{v} = 0 \ . \tag{2,3}$$

Here $A = H/R_{crucible}$ is the aspect ratio of the crucible, $Gr = g\beta(T_{hot}^* - T_{cold}^*)R_{crucible}^3/\nu^2$ the Grashof number, $Pr = \nu/\chi$ the Prandtl number, $g$ the gravity acceleration, $\beta$ the thermal expansion coefficient, and $\mathbf{e}_z$ the unit vector in the $z$-direction. The velocity boundary conditions are

$$\mathrm{v}_r = \mathrm{v}_z = 0 \ \text{at} \ \ z = 0, \ r = 1 \ \text{and} \ z = A, \ \ 0 \le r \le \eta, \ \ \eta = R_{crystal}/R_{crucible} \ , \tag{4}$$

$$\mathrm{v}_\theta = Re_{crucible} \ r \ \ \text{at} \ z = 0, \ \ \ \mathrm{v}_\theta = Re_{crucible} \ \ \text{at} \ r = 1, \tag{5}$$

$$\mathrm{v}_\theta = Re_{crystal} \ r \ \ \text{at and} \ \ z = A, \ \ 0 \le r \le \eta, \tag{6}$$

$$\mathrm{v}_z = 0, \ \ \frac{\partial \mathrm{v}_r}{\partial z} = -Ma \, Pr \frac{\partial T}{\partial r}, \ \ \frac{\partial \mathrm{v}_\theta}{\partial z} = -Ma \, Pr \frac{1}{r} \frac{\partial T}{\partial \theta} \ \ \text{at} \ z = A, \ \ \eta \le r \le 1. \tag{7}$$

Here $Ma = \gamma \left( T^*_{hot} - T^*_{cold} \right) R_{crucible} / \rho \nu \chi$ is the Marangoni number, $Re_{crystal} = \Omega_{crystal} R^2_{crucible} / \nu$, $Re_{crucible} = \Omega_{crucible} R^2_{crucible} / \nu$ are the crystal and crucible rotation Reynolds numbers, and $\gamma$ is the coefficient of the assumed linear dependence of the surface tension coefficient on the temperature. The temperature boundary conditions will be specified below, separately for each problem.

## 3. Numerical approach

   Since we are interested in the stability of steady and axisymmetric basic state $\mathbf{v} = \{U(r,z), V(r,z), W(r,z)\}$, $T(r,z)$ and $P(r,z)$ its calculation is discussed first. Assuming the rectangular staggered finite volume grid we define the scalar variables $T$ and $P$, the azimuthal velocity component $V$ and the divergence of velocity $\nabla \cdot \mathbf{v}$ at the nodes with integer indices $[r_i, z_j]$. The mesh values of the radial and axial velocity components $U$ and $W$ are defined at the points $[r_{i+1/2}, z_j]$ and $[r_i, z_{j+1/2}]$, respectively, where $r_{i+1/2} = (r_i + r_{i+1})/2$ and $z_{j+1/2} = (z_j + z_{j+1})/2$. Denoting by square brackets with subscripts $[\bullet]_{i,j}$ approximation of a term in a grid node, the resulting system of steady equations reads

$$\left[ U \frac{\partial U}{\partial r} \right]_{i+1/2, j} + \left[ W \frac{\partial U}{\partial z} \right]_{i+1/2, j} - \left[ \frac{V^2}{r} \right]_{i+1/2, j} =$$

$$= -\left[ \frac{\partial P}{\partial r} \right]_{i+1/2, j} + \left[ \frac{\partial^2 U}{\partial r^2} + \frac{1}{r} \frac{\partial U}{\partial r} - \frac{U}{r^2} + \frac{\partial^2 U}{\partial z^2} \right]_{i+1/2, j} \tag{8.1}$$

$$\left[ U \frac{\partial V}{\partial r} \right]_{i, j} + \left[ W \frac{\partial V}{\partial z} \right]_{i, j} + \left[ \frac{UV}{r} \right]_{i, j} = \left[ \frac{\partial^2 V}{\partial r^2} + \frac{1}{r} \frac{\partial V}{\partial r} - \frac{V}{r^2} + \frac{\partial^2 V}{\partial z^2} \right]_{i, j} \tag{8.2}$$

$$\left[ U \frac{\partial W}{\partial r} \right]_{i, j+1/2} + \left[ W \frac{\partial W}{\partial z} \right]_{i, j+1/2} =$$

$$= -\left[ \frac{\partial P}{\partial z} \right]_{i, j+1/2} + \left[ \frac{\partial^2 W}{\partial r^2} + \frac{\partial^2 W}{\partial z^2} \right]_{i, j+1/2} + \frac{Gr}{2} \left( T_{ij} + T_{i, j+1} \right) \tag{8.3}$$

$$\left[\frac{1}{r}\frac{\partial(rU)}{\partial r}\right]_{i,j}+\left[\frac{\partial W}{\partial z}\right]_{i,j}=0 \tag{8.4}$$

$$\left[U\frac{\partial T}{\partial r}\right]_{i,j}+\left[W\frac{\partial T}{\partial z}\right]_{i,j}=\frac{1}{Pr}\left[\frac{\partial^2 T}{\partial r^2}+\frac{\partial^2 T}{\partial z^2}\right]_{i,j} \tag{8.5}$$

The indices $i$ and $j$ vary from 1 to $N_r$ and $N_z$, respectively. To obtain the base steady axisymmetric flow the equations (8) are solved using the Jacobian-full Newton iteration. The Jacobian matrix is evaluated analytically. The computations proceed as in [125,127] using the MUMPS solver at each iteration to calculate the solution of the corresponding system of linear algebraic equations. Note that all equations (8) are solved simultaneously without any pressure-velocity decoupling. The finite volume approximations of the continuity equation (8.4) are used as equations defining the pressure.

We consider infinitesimally small three-dimensional perturbations, which are decomposed in Fourier series in the azimuthal direction. The $k$-th Fourier mode is represented as $\{\tilde{u}(x,y),\tilde{v}(x,y),\tilde{w}(x,y),\tilde{\theta}(x,y),\tilde{p}(x,y)\}\exp(\lambda t+ik\theta)$, where $\lambda$ is a complex amplification rate. It is well-known that the linear stability problem separates for each Fourier mode, so that $k$ has a meaning of an integer azimuthal wavenumber. The linear stability eigenproblem written for a calculated steady state $U$, $V$, $W$, $T$, $P$ is

$$\lambda\tilde{u}_{i+1/2,j}=-\left[U\frac{\partial\tilde{u}}{\partial r}+\tilde{u}\frac{\partial U}{\partial r}+W\frac{\partial\tilde{u}}{\partial z}+\tilde{w}\frac{\partial U}{\partial z}+\frac{ik}{r}V\tilde{u}-\frac{2V\tilde{v}}{r}\right]_{i+1/2,j}-$$
$$-\left[\frac{\partial\tilde{p}}{\partial r}\right]_{i+1/2,j}+\left[\frac{\partial^2\tilde{u}}{\partial r^2}+\frac{1}{r}\frac{\partial\tilde{u}}{\partial r}-\frac{\tilde{u}}{r^2}-\frac{k^2}{r^2}\tilde{u}+\frac{\partial^2\tilde{u}}{\partial z^2}-\frac{2ik}{r^2}\tilde{v}\right]_{i+1/2,j} \tag{9.1}$$

$$\lambda\tilde{v}_{i,j}=-\left[U\frac{\partial\tilde{v}}{\partial r}+\tilde{u}\frac{\partial V}{\partial r}+W\frac{\partial\tilde{v}}{\partial z}+\tilde{w}\frac{\partial V}{\partial z}+\frac{ik}{r}V\tilde{v}+\frac{U\tilde{v}+V\tilde{u}}{r}\right]_{i,j}-$$
$$-\left[\frac{im}{r}\tilde{p}\right]_{i,j}+\left[\frac{\partial^2\tilde{v}}{\partial r^2}+\frac{1}{r}\frac{\partial\tilde{v}}{\partial r}-\frac{\tilde{v}}{r^2}-\frac{k^2}{r^2}\tilde{v}+\frac{\partial^2\tilde{v}}{\partial z^2}+\frac{2ik}{r^2}\tilde{u}\right]_{i,j} \tag{9.2}$$

$$\lambda\tilde{w}_{i,j+1/2}=-\left[U\frac{\partial\tilde{w}}{\partial r}+\tilde{u}\frac{\partial W}{\partial r}+W\frac{\partial\tilde{w}}{\partial z}+\tilde{w}\frac{\partial W}{\partial z}+\frac{ik}{r}V\tilde{w}\right]_{i,j+1/2}$$
$$-\left[\frac{\partial\tilde{p}}{\partial z}\right]_{i,j+1/2}+\left[\frac{\partial^2\tilde{w}}{\partial r^2}+\frac{1}{r}\frac{\partial\tilde{w}}{\partial r}-\frac{k^2}{r^2}\tilde{w}+\frac{\partial^2\tilde{w}}{\partial z^2}\right]_{i,j+1/2}+\frac{Gr}{2}\left(\tilde{\theta}_{ij}+\tilde{\theta}_{i,j+1}\right) \tag{9.3}$$

$$0=\left[\frac{\partial\tilde{u}}{\partial r}+\frac{\tilde{u}}{r}+\frac{ik}{r}\tilde{v}+\frac{\partial\tilde{w}}{\partial z}\right]_{i,j} \tag{9.4}$$

$$\lambda \widetilde{\theta}_{i,j} = -\left[ U \frac{\partial \widetilde{\theta}}{\partial r} + u \frac{\partial T}{\partial r} + W \frac{\partial \widetilde{\theta}}{\partial z} + w \frac{\partial T}{\partial z} + \frac{ik}{r} V \widetilde{\theta} \right]_{i,j} +$$

$$+ \frac{1}{\Pr} \left[ \frac{\partial^2 \widetilde{\theta}}{\partial r^2} + \frac{1}{r} \frac{\partial \widetilde{\theta}}{\partial r} - \frac{k^2}{r^2} \widetilde{\theta} + \frac{\partial^2 \widetilde{\theta}}{\partial z^2} \right]_{i,j}$$

(9.5)

Assuming that **J** is the Jacobian matrix calculated from the r.h.s. of (9) and **B** is the diagonal matrix such that its diagonal elements corresponding to the values of $\widetilde{u}, \widetilde{v}, \widetilde{w}, \widetilde{\theta}$ are equal to one, while the elements corresponding to $\widetilde{p}$ are zeros, the equations (9) can be written in the matrix form as

$$\lambda \mathbf{B} \begin{pmatrix} \widetilde{u}, & \widetilde{v}, & \widetilde{w}, & \widetilde{p} & \widetilde{\theta} \end{pmatrix}^T = \mathbf{J} \begin{pmatrix} \widetilde{u}, & \widetilde{v}, & \widetilde{w}, & \widetilde{p} & \widetilde{\theta} \end{pmatrix}^T .$$

(10)

Since det**B** = 0 the generalized eigenproblem (10) cannot be transformed into a standard eigenproblem.

The stability of an axisymmetric steady flow state for a given set of the governing parameters is defined by the eigenvalue $\lambda$ having the largest real part for all integer azimuthal wavenumbers *k*. This $\lambda$ is called leading eigenvalue. Apparently, $\Lambda = \max_k \{ Real[\lambda(k)] \} > 0$ means the exponential growth of a perturbation, i.e., the instability of an axisymmetric steady flow state. The value of the azimuthal wavenumber yielding the maximum of *Real*($\lambda$) we call critical and denote as $k_{cr}$. The imaginary part of the leading eigenvalue we call critical frequency and denote as $\omega_{cr} = \mathrm{Im}[\lambda(k_{cr})]$. The corresponding eigenvector of (10) defines the meridional pattern of the most unstable perturbation of the base state.

The eigenproblem (10) is solved by the Arnoldi iteration in the shift-and-invert mode

$$(\mathbf{J} - \sigma \mathbf{B})^{-1} \mathbf{B} \begin{pmatrix} \widetilde{u}, & \widetilde{v}, & \widetilde{w}, & \widetilde{p} & \widetilde{\theta} \end{pmatrix}^T = \mu \begin{pmatrix} \widetilde{u}, & \widetilde{v}, & \widetilde{w}, & \widetilde{p} & \widetilde{\theta} \end{pmatrix}^T , \quad \mu = \frac{1}{\lambda - \sigma}$$

(11)

where $\sigma$ is a complex shift. The ARPACK package is used. To calculate the leading eigenvalue $\lambda$ it is necessary to choose the shift $\sigma$ close to $\lambda$ and to calculate 10-20 eigenvalues $\mu$ with the largest absolute value. The choice of $\sigma$ is not an easy task, since the estimate of $\lambda$ is not known. To find the leading eigenvalue we fix *Real*($\sigma$)=0 and vary *Im*($\sigma$) until the leading eigenvalue $\lambda$ is computed. Then we calculate the instability point with $\sigma = (0, Im(\lambda))$ and vary *Im*($\sigma$) further to ensure that there is no another eigenvalue with larger real part.

The computations proceed similarly to ones described in [125,127]. At the first stage we calculate a steady axisymmetric flow state using the Jacobian-

full exact Newton iteration. Then the linear stability of the calculated steady flow is studied for each value of $k$ separately. For each $k$ we compute the marginal value of the critical parameter, which can be Reynolds, Grashof, or Marangoni number, or other. The marginal value is computed by solving the equation $max\ [Real(\lambda)] = 0$ for a fixed $k$ using the secant method. All other parameters during these computations are fixed. The minimum of the marginal values over all $k$ yields the value of the critical parameter corresponding to the instability of the base flow.

As it was done in [125, 127] we combine both Newton and Arnoldi iteration techniques with the multifrontal direct solvers for sparse matrices (we use the MUMPS solver). The efficiency of this approach is a sequence of the high level of sparseness of the Jacobian matrices of equations (8) and (9). Using the second-order finite volume discretization scheme these matrices are composed from banded blocks of the size $(N_r \times N_z) \times (N_r \times N_z)$, where each block have less than 15 diagonals filled by non-zero elements. The **LU-**decomposition of the matrix (**J** - $\sigma$**B**) remains unchanged for the whole Arnoldi iteration procedure, which makes the iterations much faster than it is observed in the cases when Krylov-subspace-based iterative solvers are applied. For the Newton iteration the efficiency of such approach is not obvious, but appears to be rather good. The characteristic times needed for the calculation of a steady state and for performing the stability analysis can be found in the Appendix of [127].

# 4. Validation of the code

It should be mentioned that there is no well-established experimental or numerical data, which allows for a complete and certain validation of a code of such complexity. The set of benchmarks formulated for much simpler configurations was considered in [125, 127]. Here we report comparisons with the experiments [19] and with the calculation of the eigenvalues made in [121,122]. Then we address the configuration of experiments [35], and show how the critical parameters calculated for this configuration converge on uniform and stretched grids.

The model experiments [19] were carried out in isothermal cylindrical crucible with an isothermal crystal dummy using silicone oil with $Pr = 1000$ as a working liquid. Apparently, this Prandtl number is too large to characterize even relatively large Prandtl number oxide melts, for which it usually does not exceed the value of 20. On the other hand this is the only experimental study of the Czochralski melt flow we could find where the critical parameters were measured and the boundary conditions were controlled precisely enough to make it possible to compare with calculations. In these experiments the temperature drop between the crystal and the crucible was fixed and the rotation of both crystal and crucible was varied. Figure 2 shows the measured and
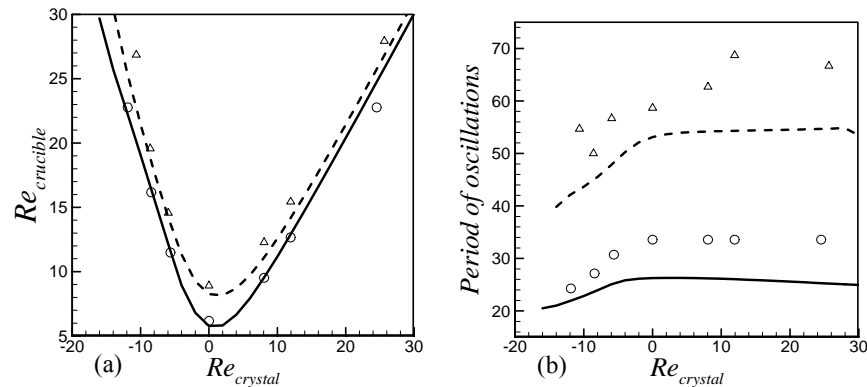
**Figure 2.** Critical value of the crucible rotation Reynolds number (a) and period of appearing oscillations (b) versus the crystal rotation Reynolds number. Symbols correspond to the experiments of Munakata & Tanasawa [19] and lines to present calculations. Solid line and ○ for *Gr* = 356, *Ma* = 1660; Dashed line and ∆ for *Gr* = 1020, *Ma* = 4756.

calculated values of the critical crucible Reynolds number and the corresponding period of oscillations for different crystal rotation rates and for two different heating conditions (see figure caption). The instability in this case is axisymmetric ($k = 0$), which is consistent also with the experimental and numerical observations of [28] made for large-Prandtl-number fluids. Figure 1a shows that the experimental and calculated critical Reynolds numbers agree very well. An examination of Fig. 2b shows that our calculations reproduce a correct tendency of variation of the oscillation period, however there is no a precise agreement, like in Fig. 2a. This discrepancy can be explained by the fact that the experimental values of the period are measured at some finite supercriticality while the calculation yields this value exactly at the instability point. The difference can be larger in the case of subcritical bifurcation, however the issue of sub- or supercriticality is not considered here. Another possibility is not very precise values of the thermophysical parameters given in [19], which prevent a correct transformation of dimensionless results into dimensional ones. Since the instability is axisymmetric the time-dependent axisymmetric calculations performed in [19] also showed rather good agreement with experiment. Comparing to the present results the critical numbers were slightly overestimated and the critical periods showed a similar discrepancy.

The next comparison was made for the eigenvalues of the linearized equations (9) computed in [121,122]. A model problem similar to one considered here was studied in these works. The bottom of a cylindrical crucible was assumed to be thermally insulated and the sidewall to be isothermal. It was assumed also that there exists a linear temperature profile at the free melt surface, which would correspond to a very large heat conductivity

**Table 1.** Eigenvalues calculated for the data of Nikitin & Polezhaev [121, 122] using defferent finite volume grids. $Gr = 10^6$.

| $k$ | 100×100 | 200×200 | 300×300 | 400×400 | 500×500 | Result of [122] |
|---|---|---|---|---|---|---|
| | | | $Re_{crystal} = 0$ | | | |
| 1 | (-46.99, 808.6) | (-49.21, 811.1) | (-49.69, 811.6) | (-49.86, 811.8) | (49.94, 811.8) | (-54., 795.) |
| 2 | (-70.27, 223.0) | (-68.91, 223.2) | (-68.69, 223.3) | (-68.61, 223.3) | (-68.59, 223.3) | (-80., 247.) |
| 3 | (56.63, 485.8) | (57.88, 488.8) | (58.11, 489.3) | (58.18, 489.5) | (58.22, 489.6) | (48., 478.) |
| 4 | (50.55, 993.3) | (50.39, 997.4) | (50.32, 998.2) | (50.28, 998.5) | (50.26, 998.6) | (38., 966.) |
| 5 | (-55.11, 1039.) | (-56.01, 1046.) | (-56.11, 1047.) | (-56.15, 1047.) | (-56.18, 1048.) | (-68., 1030.) |
| 6 | (-25.18, 0) | (-26.91, 0) | (-27.29, 0) | (-27.43, 0) | (-27.50, 0) | (-39., 424.) |
| | | | $Re_{crystal} = 1000$ | | | |
| 1 | (-24.60, -807.3) | (-31.49,- 809.2) | (-33.11, -809.3) | (-33.79, -809.2) | (-34.16, -809.1) | (214., -2130.) |
| 2 | (-64.71, -1201.) | (-66.16, -1208.) | (-66.55, -1210.) | (-66.72, -1210.) | (-66.81, -1211) | (-95., -) |
| 3 | (64.23, -566.9) | (64.48, -572.0) | (64.38, -573.4) | (64.30, -574.0) | (64.24, -574.3) | (58., 58) |
| 4 | (29.17, -1056.) | (26.93, -1061.) | (26.14, -1062.) | (25.75, -1062.) | (25.53, -1062). | (-13., -) |
| 5 | (-26.70, -1114.) | (-27.90, -1122.) | (-28.18, -1124.) | (-28.31, -1125.) | (-28.38, -1125.) | (-42., -) |
| 6 | (-83.57, -974.2) | (-88.13, -977.5) | (-89.86, -978.6) | (-90.72, -979.1) | (-91.23, -979.4) | (-88., -) |

of the melt. Steady states and the corresponding eigenvalues were computed for $A$=1, $Pr$=0.05, $Ma$=0, $Re_{crystal}$=0 and 1000, $Re_{crucible}$=0 and $Gr$=$10^5$, $5\times10^5$, and $10^6$. The azimuthal wavenumber $k$ was varied from 1 to 6. The calculations of [121,122] were unsteady and three-dimensional using the finite difference method in the ($r,z$) plane and the pseudospectral approach in the azimuthal direction. The finest grid in the meridional plane had 128×128 nodes. The eigenvalues were calculated from the calculated time-dependent perturbation amplitudes. We repeated this calculation using different finite volume grids with the number of nodes in one direction varied from 100 to 500 and with the direct calculation of the eigenvalues. The results are reported in Table 1. It is seen that present results converge with the grid refinement, however the convergence rate is different for different $Re_{crystal}$ and azimuthal wavenumbers. The difference is caused by the different spatial patterns of the corresponding eigenvectors, which are not shown here. Comparison with the results of [121,122] shows only a qualitative agreement. In the author's opinion the present calculations are more accurate and the comparison indicates on two important numerical issues: the grid convergence, which needs more than 100 nodes in the shortest spatial direction (see also [125,127]), and on the importance of correct calculations of the eigenvalues, which cannot be extracted from time-dependencies accurately enough.
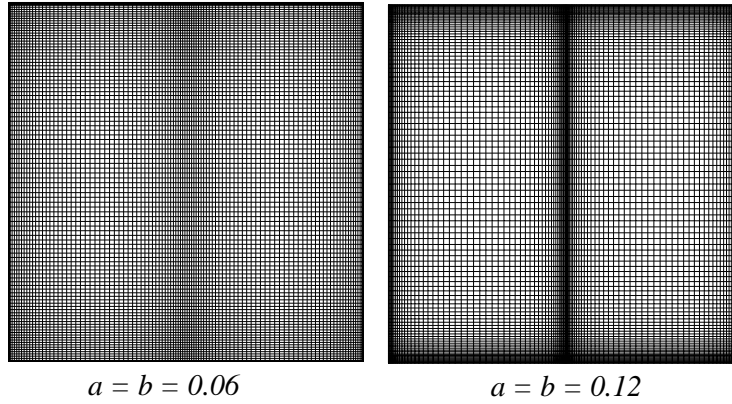
$a = b = 0.06$                                        $a = b = 0.12$

**Figure 3.** Examples of the grid stretching.

In the next example illustrated in Figs. 3 and 4 we illustrate the convergence of critical temperature difference and the critical frequency for the example described in the Section 5 below. Here we are interested in the rate of convergence and the effect of mesh stretching. The mesh stretching is a rather unclear issue. The common opinion is that the stretching improves the convergence, however, as it was shown in [125,127], it is not always the case. It is not quite clear also where the stretching should be applied for the model considered here. In this study we tried to stretch the grid near the boundaries, near the cylindrical axis and also near the discontinuity point $r = R_{crystal}, z = A$, where the crystal meets the melt surface. The stretching used here is defined in the following way:

$$\text{for } 0 \leq r \leq R_{crystal}: \quad r_i \leftarrow r_i - a\,sin\left(2\pi \frac{r_i}{R_{crystal}}\right) \tag{9.1}$$

$$\text{for } R_{crystal} \leq r \leq R_{crucible}: \quad r_i \leftarrow r_i - \left(1 - R_{crystal}\right)a\,sin\left(2\pi \frac{r_i - R_{crystal}}{1 - R_{crystal}}\right) \tag{9.2}$$

$$z_j \leftarrow A\left[\frac{z_j}{A} - b\,sin\left(2\pi \frac{z_j}{A}\right)\right] \tag{9.3}$$

where parameters $a$ and $b$ vary from 0 to 0.12. Apparently $a = b = 0$ corresponds to the uniform grid. Examples of the stretched grids are given in Fig. 3.

Taking the configuration of a model experiment of [35] as a representative example we calculated the critical temperature difference and the critical frequency of oscillations for the stationary crystal and the crystal rotation Reynolds number equal to 1000 and 5000. The calculations were done using the
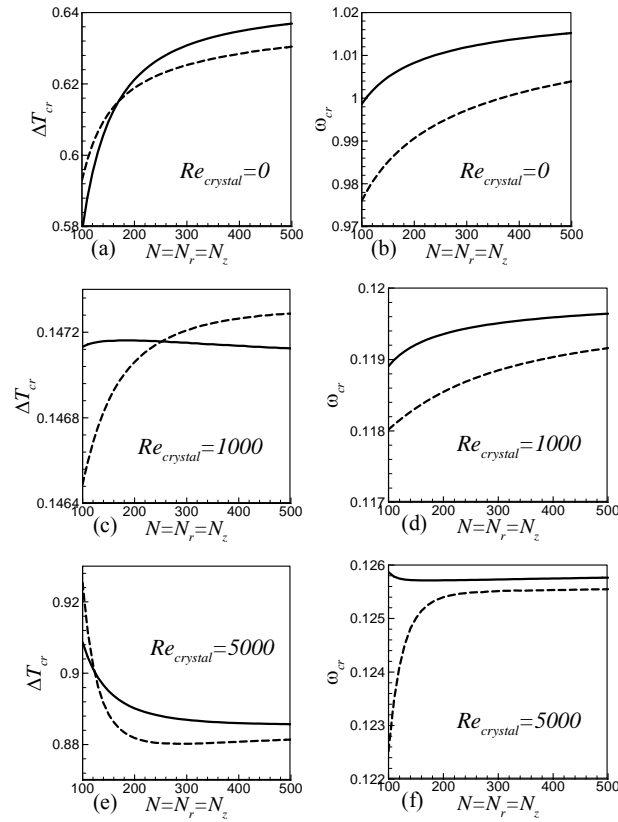
**Figure 4.** Convergence of the critical temperature difference and the critical frequency for different crucible rotation rates. Results for the configuration of [35]. Dash line – uniform grid, solid line – stretched grid with $a = b = 0.12$.

uniform and stretched grids with the number of nodes in both $r$- and $z$-directions varied from 100 to 500 with the increment of 10. Note that at $Re_{crystal} = 0$ the instability sets in as a transition to an axisymmetric oscillatory state ($k = 0$), while at $Re_{crystal} = 1000$ and 5000 an azimuthal traveling wave with the azimuthal wavenumber $k = 1$ breaks the axial symmetry.

Figure 4 shows that unlikely simpler benchmark problems [125,127] the definite convergence is not reached even with the use of the grid of $500^2$ nodes. We can state that the largest discrepancy between the uniform at stretched grids at $N = N_r = N_z = 500$ is observed for the critical frequency calculated for $Re_{crystal} = 0$, where it reaches approximately 1% (Fig. 4f). The uniform grid exhibits the fastest convergence at $Re_{crystal} = 1000$. It is striking that starting from this Reynolds number the calculations with the stretched grid converge visibly faster. Starting from approximately $N = 300$ both stretched and uniform grids yield rather reliable results with the accuracy sufficient for the practical purposes. On the other hand, use of the grids coarser than 100×100, especially without stretching, can lead to a significant inaccuracy. The calculations reported below are carried out on the 300×300 grid.

**Table 2.** Comparison of the critical temperature difference and critical frequency calculated on uniform and stretched grids and their Richardson extrapolations.

| $Re_{crystal}$ | 0 | 1000 | 5000 | 0 | 1000 | 5000 |
|---|---|---|---|---|---|---|
| | $\Delta T_{cr}$ | | | $\omega_{cr}$ | | |
| Uniform grid, 500×500 | 0.63046 | 0.14729 | 0.88142 | 1.0039 | 0.11916 | 0.12555 |
| Richardson extrapolation from uniform grid | 0.63562 | 0.14734 | 0.88286 | 1.0098 | 0.11940 | 0.12558 |
| Stretched grid, 500×500 | 0.63690 | 0.14712 | 0.88572 | 1.0152 | 0.11964 | 0.12576 |
| Richardson extrapolation from stretched grid | 0.64099 | 0.14708 | 0.88531 | 1.0178 | 0.11975 | 0.12581 |

It was argued in [127] that Richardson extrapolation improves the results even for problems having discontinuous boundary conditions, for which local convergence of the Taylor series cannot be expected. It is not easy to check this statement for the present case, since no reference solution exists. We expect that if the Richardson extrapolation is helpful then the results extrapolated from the uniform and stretched grids will become closer. We checked that by calculation of the Richardson extrapolation based on $490^2$ and $500^2$ grids. The results are shown in Table 2, from which we can conclude that the Richardson extrapolations based on the stretched and uniform grids are really closer than the results corresponding to calculation of the $500^2$ grid.

To present an example of an insufficient resolution we consider configuration of [85,86]. The melt flow of LiNbO₃ ($Pr = 13.6$) in the crucible with the aspect ratio $A = 1.945$ is considered. The bottom of the crucible is thermally insulated and the heat is supplied through the sidewall with a constant heat flux $q$. The governing parameter characterizing the heating is the dimensionless heat flux $Q = qR_{crucible}/\kappa\Delta T$. The melt surface is cooled by radiation, which is characterized by the dimensionless parameter $Rd = \sigma\varepsilon\Delta T^3 R_{crucible}/\kappa$ and dimensionless ambient temperature $\theta_a$. Here $\chi$ is the thermal conductivity, $\sigma$ is the Stefan-Boltzmann constant and $\varepsilon$ is the emissivity. Since there is no characteristic temperature difference in this case we follow [85,86] and choose $\Delta T = T_{melting} = 1526\ K$. For the example we use parameters of Fig. 8 of [86], which are $Q = 0.05$, $Rd = 0.34$ and $\theta_a = 0.8$, $Re_{crystal} = Re_{crucible} = 0$.

The first unexpected result for the above parameters is the existence of two distinct steady states of the flow. They are illustrated in Fig. 5. The first branch (two left frames of Fig. 5) is the one obtained in [86]. The second branch (two right frames in Fig. 5) can be called "anomalous" since its minimal temperature is below the melting point, which would mean that part of the flow region can be frozen. On the other hand, as it is shown below, this branch is always unstable
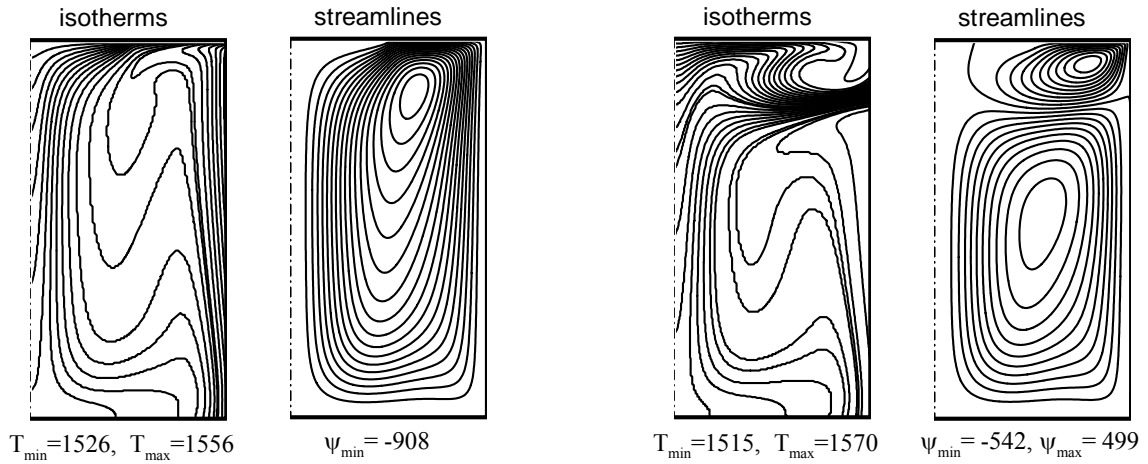
| isotherms | streamlines | isotherms | streamlines |
|---|---|---|---|



$T_{min}$=1526, $T_{max}$=1556        $\psi_{min}$= -908        $T_{min}$=1515, $T_{max}$=1570        $\psi_{min}$= -542, $\psi_{max}$= 499

**Figure 5.** Two steady states corresponding to configuration of [85,86].

and it is not quite clear how the instability will develop if this steady axisymmetric solution will be supplied to a three-dimensional solver as an initial condition.

Tables 3 and 4 show how the real part of the leading eigenvalue converges with the grid refinement. For this exercise we varied the azimuthal wavenumber $k$ from 0 to 10 and used stretched grids with $a = b = 0.12$. Considering the first branch (two left frames in Fig. 5 and Table 3) we see that a qualitatively correct result, i.e., the eigenvalue and the eigenvector describing the most unstable perturbation, are obtained starting from the grid consisting of 60×60 nodes in the meridional plane. Coarser grids of 40×40 and 50×50 nodes can lead to a wrong conclusion that the flow is unstable. The calculations of [85,86] used not more than 40×40 nodes in the azimuthal plane, which really lead to observation of the axisymmetry-breaking and three-dimensional flow patterns. According to the present result these observations are caused by a numerical inaccuracy.

The second steady state branch (two right frames in Fig. 5 and Table 4) is always unstable for the considered values of parameters. However, an examination of the convergence shown in Table 4 shows that a qualitatively correct answer for this case can be obtained only starting from 100×100 nodes grid. Presumably, the slower convergence is a consequence of a more complicated flow structure (see Fig. 5). We see also that a certain conclusion about the convergence cannot be made on the basis of another similar case, but the convergence needs to be studied separately every time.

The stability study of the first steady state branch shows that for the crystal Reynolds number varied from 0 to 200 it becomes unstable due to the azimuthal modes $k = 1$ and 2 and the critical dimensionless heat flux varies from $Q_{cr} = 3.7$ at $Re_{crystal} = 0$ to $Q_{cr} = 2.7$ at $Re_{crystal} = 200$.

**Table 3.** Convergence of Real($\lambda_k$) for the first steady state branch of the configuration of [85,86] (two left frames of Fig. 5).

| $N_r \times N_z$ | $k=0$ | $k=1$ | $k=2$ | $k=3$ | $k=4$ | $k=5$ | $k=6$ | $k=7$ | $k=8$ | $k=9$ | $k=10$ |
|---|---|---|---|---|---|---|---|---|---|---|---|
| 40×40 | 0.07353 | 0.07355 | 0.07360 | 0.07367 | 0.07377 | 0.07389 | 0.07402 | 0.07414 | 0.07423 | 0.07427 | 0.07427 |
| 50×50 | -0.4793E-3 | -0.01202 | 0.07360 | 0.04164 | 0.04127 | 0.04077 | 0.04014 | 0.03938 | 0.03848 | 0.03741 | 0.03617 |
| 60×60 | -0.44423E-3 | -0.01210 | -0.01846 | -0.01894 | -0.02022 | -0.02278 | -0.02512 | -0.02650 | -0.02811 | -0.02997 | -0.03208 |
| 80×80 | -0.4485E-3 | -0.01217 | -0.01851 | -0.01896 | -0.02023 | -0.02279 | -0.02641 | -0.02901 | -0.03058 | -0.03259 | -0.03506 |
| 100×100 | -0.4527E-3 | -0.01220 | -0.01854 | -0.01897 | -0.02023 | -0.02280 | -0.02643 | -0.02905 | -0.03062 | -0.03262 | -0.03509 |
| 120×120 | -0.4556E-3 | -0.01221 | -0.01856 | -0.01898 | -0.02023 | -0.02280 | -0.02644 | -0.02909 | -0.03065 | -0.03265 | -0.03512 |
| 140×140 | -0.4583E-3 | -0.01221 | -0.01857 | -0.01898 | -0.02023 | -0.02280 | -0.02645 | -0.02912 | -0.03068 | -0.03268 | -0.03513 |
| 160×160 | -0.4602E-3 | -0.01222 | -0.01858 | -0.01899 | -0.02023 | -0.02280 | -0.02645 | -0.02915 | -0.03070 | -0.03270 | -0.03515 |
| 180×180 | -0.4618E-3 | -0.01221 | -0.01858 | -0.01899 | -0.02023 | -0.02280 | -0.02646 | -0.02917 | -0.03072 | -0.03272 | -0.03517 |
| 200×200 | -0.4632E-3 | -0.01221 | -0.01859 | -0.01899 | -0.02023 | -0.02280 | -0.02646 | -0.02919 | -0.03074 | -0.03273 | -0.03518 |

**Table 4.** Convergence of Real($\lambda_k$) for the second steady state branch of the configuration of [85,86] (two right frames of Fig. 5).

| $N_r \times N_z$ | k = 0 | k = 1 | k = 2 | k = 3 | k = 4 | k = 5 | k = 6 | k = 7 | k = 8 | k = 9 | k = 10 |
|---|---|---|---|---|---|---|---|---|---|---|---|
| 40×40 | 0.03064 | 0.03076 | 0.06420 | 0.05845 | 0.05240 | 0.04637 | 0.04094 | 0.03599 | 0.03570 | 0.03637 | 0.03689 |
| 60×60 | 0.003920 | 0.3747e-4 | -0.01448 | 0.07153 | 0.1444 | 0.3078 | 0.3072 | 0.3060 | 0.3043 | 0.3018 | 0.2985 |
| 80×80 | 0.002580 | 0.09510 | 0.09116 | 0.08589 | 0.2370 | 0.2336 | 0.2295 | 0.2245 | 0.2188 | 0.2121 | 0.2046 |
| 100×100 | 0.2204 | 0.2198 | 0.2180 | 0.2154 | 0.2121 | 0.2081 | 0.2035 | 0.1981 | 0.1920 | 0.1851 | 0.1174 |
| 120×120 | 0.2098 | 0.2092 | 0.2072 | 0.2042 | 0.2006 | 0.1963 | 0.1913 | 0.1857 | 0.1794 | 0.1724 | 0.1647 |
| 140×140 | 0.2040 | 0.2033 | 0.2011 | 0.1979 | 0.1941 | 0.1896 | 0.1845 | 0.1787 | 0.1723 | 0.1652 | 0.1574 |
| 160×160 | 0.2004 | 0.1996 | 0.1973 | 0.1940 | 0.1901 | 0.1855 | 0.1802 | 0.1743 | 0.1678 | 0.1607 | 0.1529 |
| 180×180 | 0.1980 | 0.1972 | 0.1948 | 0.1914 | 0.1874 | 0.1827 | 0.1774 | 0.1714 | 0.1649 | 0.1577 | 0.1498 |
| 200×200 | 0.1963 | 0.1955 | 0.1931 | 0.1896 | 0.1855 | 0.1807 | 0.1753 | 0.1693 | 0.1627 | 0.1555 | 0.1477 |

# 5. Results

As mentioned above, we use the experimental configuration of [35] for a representative study of three-dimensional instability of axisymmetric melt flows. We consider the flow of $NaNO_3$ melt with $Pr = 9.2$ in the crucible of the aspect ratio height/radius = 0.92 and the crystal to crucible radii ratio 0.5 . The temperature boundary conditions are defined as

$T = T_{hot}$ at the crucible sidewall; $T = T_{melting}$ at the melt/crystal interface;          (10)

$$T = T_{hot}\left(0.8571 + 0.1429\left(\frac{r}{R_{crucible}}\right)^2\right) \text{ at the crucible bottom;}$$          (11)

$$\frac{\partial T}{\partial z} = -Bi\left(T - T_{melting}\right) \text{ at the free surface}$$          (12)

Defining $\Delta T = T_{hot}$ - $T_{melting}$ and using the data of [35] we estimate the Grashof and Marangoni numbers as $Gr = 1.9 \times 10^5 \, \Delta T$ and $Ma = 5400 \, \Delta T$, where $\Delta T$ is measured in $^{o}C$. The Biot number is fixed and is estimated as $Bi = 0.1$  Since a variation of temperature difference $\Delta T$ affects both Grashof and Marangoni numbers in the following we consider as a critical parameter the temperature difference itself, and not one of the dimensionless numbers. Such a consideration makes it easier to connect our numerical results with possible future experiments.

An example of the marginal stability curves showing the dependence of the marginal value of the temperature difference $\Delta T_k$ on the crystal rotation Reynolds number $Re_{crystal}$ for the stationary crucible is shown in Fig. 6. The marginal temperature difference $\Delta T_k$ corresponds to the beginning of growth of the perturbations with a fixed $k$ ($k = 0, 1$ and 2 in Fig. 6). The largest value of the crystal rotation Reynolds number considered is 5000, which for the experimental data of [35] corresponds to the rotation frequency of approximately 0.8 rps. This rotation rate seems to be too large for the Czochralski setup, however it can be easily reached at smaller viscosities or larger crystal or crucible radii.

As explained above, the onset of instability corresponds to the minimum of $\Delta T_k$ over all values of $k$. The values of $\Delta T_k$ for $k > 2$ were always larger than the values plotted in Fig. 6. At the same time with the increase of the crystal rotation the axisymmetric mode $k = 0$ and the three-dimensional mode $k = 1$ yield the minimum of $\Delta T_k$ and several times replace each other as critical modes. For $Re_{crystal} > 1000$ the mode $k = 2$ has the marginal values of $\Delta T$ close to the critical ones. This can lead to an interaction of the two or even three modes in the supercritical regime, which would mean a rather complex non-linear
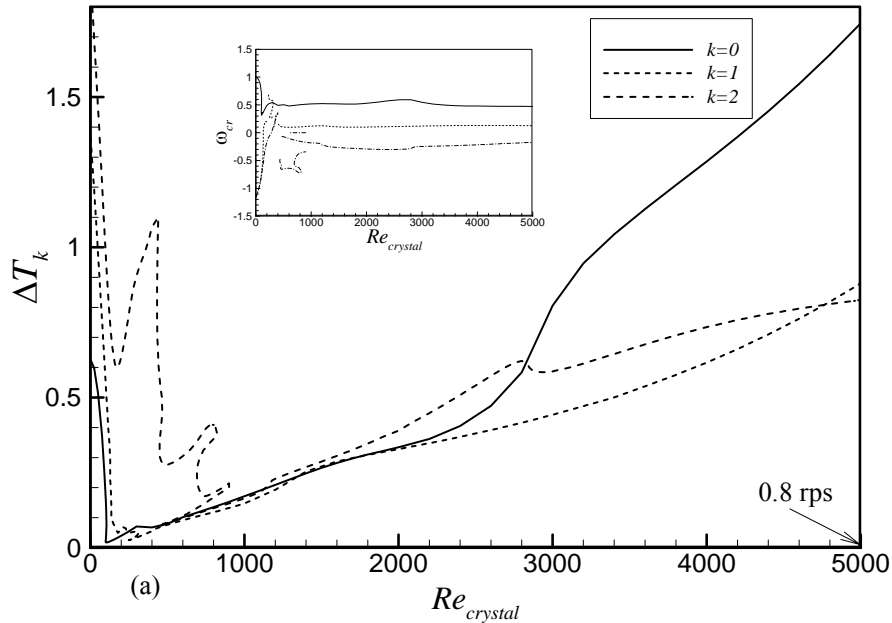
**Figure 6.** Marginal temperature difference and critical frequency for the three-dimensional instability of flow configuration of [35]. $Re_{crucible} = 0$.

dynamics. Note also a sharp decrease of the critical value of $\Delta T$ with a very weak increase of the rotation rate from the zero value. Such a destabilization was observed also in [21,22,74,126] and in our calculations, which are not included in this paper. It seems to be a common feature for the melts with $Pr > 1$. Attempts to explain the physics of this destabilization were done in the above cited papers, however the comprehensive explanation is yet to be done.

The marginal frequencies of oscillations corresponding to the marginal stability curves of Fig. 6 are shown in the insert. Note that the negative value of the critical frequency means that the unstable azimuthal traveling wave rotates in the direction opposite to the crystal rotation. It is seen that the frequencies corresponding to the different modes have different signs and magnitude, which also can make their interaction very complicated.

To illustrate how different can be flow patterns and the perturbations leading to instability we illustrate some of them in Figs. 7 and 8. Figure 7 shows two cases that correspond to the axisymmetric instability at $k = 0$, and Fig. 8 other two cases corresponding to $k = 1$. It is seen that the instability at $Re_{crystal} = 0$ is developing near the cylindrical axis (left border of the graphs). When rotation is relatively strong, at $Re_{crystal} \geq 1000$, the perturbation amplitude is distributed over the whole flow region, however its pattern undergoes noticeable changes. Apparently, an additional and considerable effort is needed to describe the physical mechanisms, which cause the instability and to gain the understanding of the rapid destabilization of the flow at small crystal rotation rates.

Several studies [19,54-61,94,117,120] describe a possibility to affect the melt flow instability by a simultaneous rotation of the crystal and crucible. For the configuration considered here this possibility is shown in Fig. 9 for two fixed crucible Reynolds numbers 100 and −100, which correspond to the co- and counter-rotating crucible, respectively. For the data of [35] this value of the Reynolds number can be reached with the crucible angular velocity of approximately 2 rpm. The flow is stable inside the neutral stability lines plotted in Figs. 9a and 9b and unstable outside of them. The striking observation is that by a slow crucible rotation the critical temperature difference can be increased in several times or even in an order of magnitude compared with the stability limit corresponding to the stationary crucible. Our calculations show that the patterns of meridional flow do not change significantly when the crucible rotates with $Re_{crucible} = \pm100$ or is stationary. At the same time the stability properties of the flows illustrated in Fig. 9 change drastically (cf. Fig. 9 and Fig. 6). Clearly, this stabilization effect is different for different configurations, however its existence is obvious and can be used in the crystal growth processes. The comprehensive explanation of this stabilization is not given yet and possibly has to be done in a framework of a fundamental fluid dynamics research.
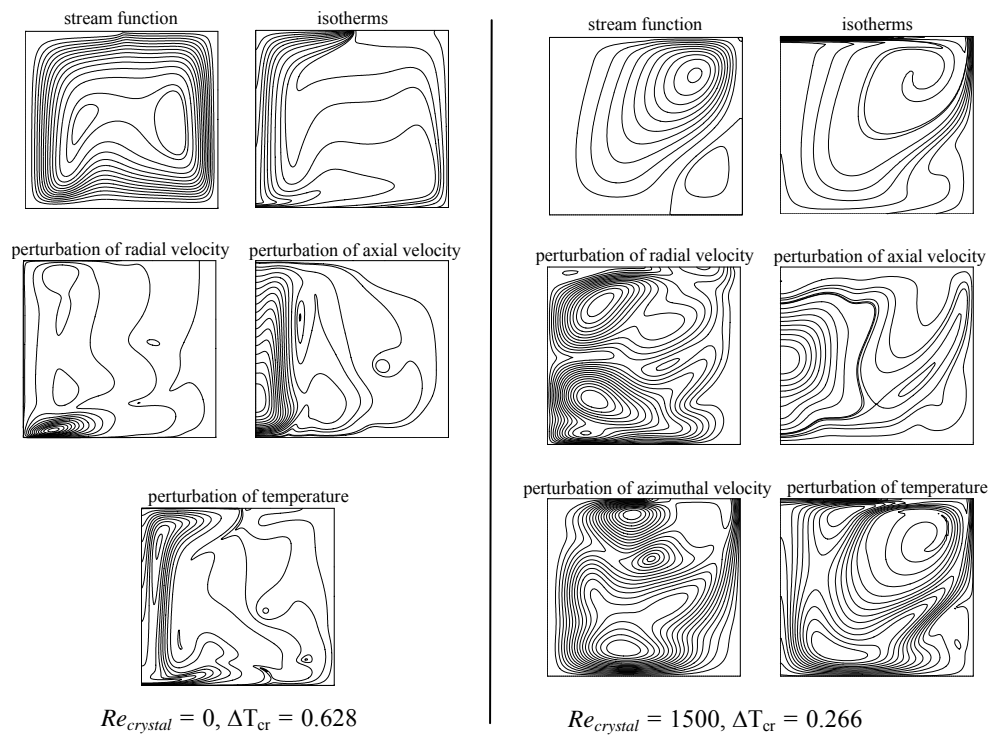


$Re_{crystal} = 0, \Delta T_{cr} = 0.628$          $Re_{crystal} = 1500, \Delta T_{cr} = 0.266$

**Figure 7.** Patterns of flows at the critical points and patterns of the perturbation amplitudes for the instability corresponding to the axisymmetric mode $k = 0$. $Re_{crucible} = 0$.
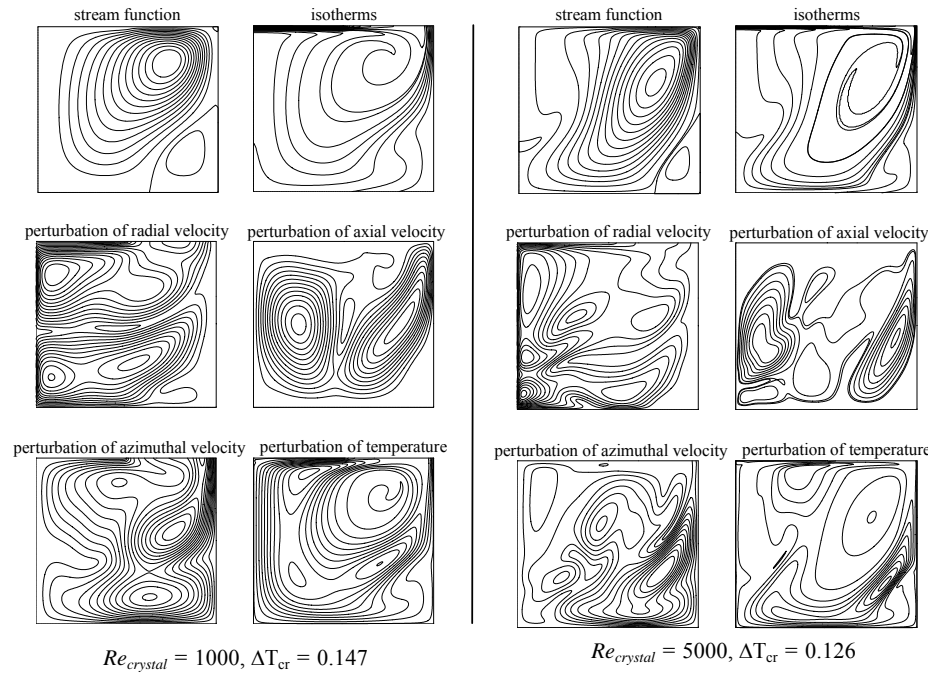
| stream function | isotherms | | stream function | isotherms |

perturbation of radial velocity | perturbation of axial velocity

perturbation of azimuthal velocity | perturbation of temperature

$Re_{crystal}$ = 1000, $\Delta T_{cr}$ = 0.147          $Re_{crystal}$ = 5000, $\Delta T_{cr}$ = 0.126

**Figure 8.** Patterns of flows at the critical points and patterns of the perturbation amplitudes for the instability corresponding to the axisymmetric mode $k = 0$. $Re_{crucible} = 0$.
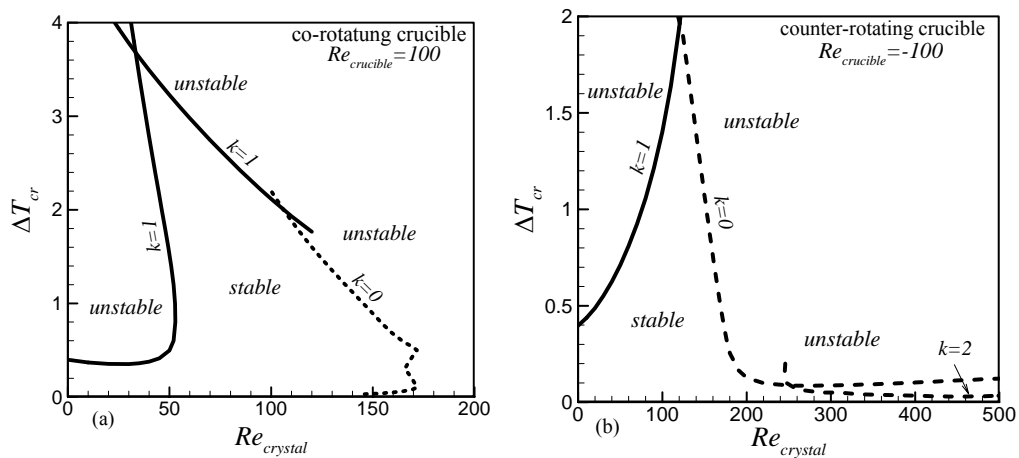


**Figure 9.** Fragments of stability diagrams for the experimental configuration of [35] calculated for a slow crucible rotation.

# 6. Concluding remarks

The three-dimensional stability analysis of the hydrodynamic model of Czochralski melt flow can be done in a realistic time on a rather moderate computer using the approach similar to one used in [125,127] for simpler benchmark problems. We have shown that the conclusion of [125,127] stating

that the convergence of the critical parameters requires finite volume grids having about 100 or mode nodes in the shortest spatial direction remains valid also for the Czochralski melt flow and even sometimes should be strengthened. The present results show that the convergence strongly depends on the governing parameters and varies for different Fourier modes. Therefore it should be examined for every configuration separately. As shown above, a insufficient numerical accuracy can lead to wrong qualitative conclusions.

The stability diagram calculated for experimental configuration of [35] showed that a slow rotation of the crystal leads to a steep decrease of the critical temperature difference. In other words a combination of a weak rotation with a weak heating destabilizes the flow. The nature of this destabilization is yet to be studied, however it seems to be a rather common phenomenon for different Czochralski systems. Another observation made is a possibility of significant flow stabilization by a slow rotation of the crucible. Again, the mechanism of this stabilization needs to be studied separately.

One of the crucial problems for the computations of this kind is a possibility to validate the code against independent calculations and experiments. Several attempts of doing this are described in this paper, however they are not sufficient. In the author's opinion it is necessary to formulate a benchmark problem based on an experiment. The experiment should be done with the sufficient control of all the boundary conditions, so that it will be possible to reproduce them in numerical models. Computations of flows and their instabilities using different numerical approaches for the problem formulated on the basis of such an experiment will yield a valuable benchmark data, necessary for the further development of computational modeling.

Future development of the current numerical approach will focus on the issues of phase transition, capillary meniscus and volume radiation in the transparent and semi-transparent melts and crystals. The latter is necessary to study the growth of oxide crystals [12]. We intend to include these effects in the steady solver and to examine their effect on the stability of melt flow.

## Acknowledgements

## References
1.    Hurle D.T.J. 1966, *Philosophical Magazine*, *13, 305.*
2.    Hurle D.T.J. 1983, *J. Cryst. Growth*, 65, 124.
3.    Hurle D.T.J. 1983, *Mater. Sci. Forum*, **276-277**, 27.
4.    Brehm C., Boniort J.-Y., Margotin P. 1973, *J. Cryst. Growth*, **18**, 191.
5.    Kim K.M., Smetana P. 1985, *J. Appl. Phys.*, **58**, 2731.

6.   Tower J.P., Tobin R., Pearah P.J., Ware R.M. 1991, *J. Cryst. Growth*, **114**, 665.
7.   Santos M.T., Rojo J.C., Cintas A., Arizmendi L., Dieguez E. 1995, *J. Cryst. Growth*, **156**, 413.
8.   Sasaura M., Miyazawa S. 1996, *J. Cryst. Growth*, **166**, 825.
9.   Kanda T., Hourai M., Miki S., Shigematsu T., Tomokage H., Miyano T., Morita H., Shintani A. 1996, *J. Cryst. Growth*, **166**, 663.
10.  Zhao G.I., Zeng X.H., Zhou S.M., Xu J., Tian Y.L., Huang W. X., 2003, *Phys. Stat. Solidi*, **199**, 186.
11.  Dold P. 2003, *Crystal Research and Technology*, **38**, 659.
12.  Uecker R., Wilke H., Schlom D.G., Velickov B., Reiche P., Polity A., Bernhagen M., Rossberg M. 2006, *J. Cryst. Growth*, **295**, 84.
13.  Gelfgat A. Yu., Bar-Yoseph P.Z. 2004, *Int. J. Numer. Meth. Heat and Fluid Flow*, **14,** 213.
14.  Lappa M. Fluids, Materials and Microgravity: Numerical Techniques and Insights into Physics, Elsevier, 2004, 520pp.
15.  Lappa M. 2005, *Cryst. Res. Technol.,* **40**, 531.
16.  Scheel H.J. 2001, *J. Cryst. Growth*, **211**, 1.
17.  Scheel H.J. In: Crystal Growth Technology (eds. H.J.Scheel and T. Fukuda), John Wiley & Sons, 2003, pp.3-14
18.  Hurle D.T.J, Cockayne B. In: *Handbook of Crystal Growth* (ed. D.T.J. Hurle), North-Holland, Amsterdam, **2**, 99.
19.  Munakata T., Tanasawa I. 1990, *J. Cryst. Growth*, **106**, 566.
20.  Ozoe H., Toh K., Inoue T., 1991, *J. Cryst. Growth*, **110**, 472.
21.  Kishida Y., Tanaka M., Esaka H. 1993, *J. Cryst. Growth*, **130**, 75.
22.  Seidl A., McCord G., Müller G., Leister H.-J. 1994, *J. Cryst. Growth*, **137**, 326.
23.  Togawa S., Chung S.-I., Kawanishi S., Izunome K., Terashima K., Kimura S. 1996, *J. Cryst. Growth*, **160**, 41.
24.  Togawa S., Chung S.-I., Kawanishi S., Izunome K., Terashima K., Kimura S. 1996, *J. Cryst. Growth*, **160**, 49.
25.  Miyano T., Inami S.-I., Shintani A., Kanda T., Hourai M. 1996, *J. Cryst. Growth*, **166**, 469.
26.  Lee Y.-S., Chun Ch.-H. 1997, *J. Cryst. Growth*, **180**, 477.
27.  Choi J.-I., Sung H.J. 1997, *Int. J. Heat Mass Transfer*, **40**, 1667.
28.  Choi J.-I., Kim S., Sung H.J., Nakano A., Koyama H.S. 1997, *J. Cryst. Growth*, **180**, 305.
29.  Lee Y.-S., Chun Ch.-H. 1999, *J. Cryst. Growth*, **197**, 297.
30.  Lee Y.-S., Chun Ch.-H. 1999, *J. Cryst. Growth*, **197**, 307.
31.  Hintz P., Schwabe D., Wilke H. 2001, *J. Cryst. Growth*, **222**, 343.
32.  Hintz P., Schwabe D. 2001, *J. Cryst. Growth*, **222**, 356.
33.  Schwabe D., 2002, , *J. Cryst. Growth*, **239**, 1849.
34.  Hibiya T., Azami T., Sumiji M., Nakamura S., 2003: in: *Interfacial Fluid Dynamics and Transport Process"*, Narayanan, R., Scwabe, D., (Eds), Springer, New York, 2003, pp. 131-155.
35.  Schwabe D., Sumathi R.R., Wilke H. 2004, *J. Cryst. Growth*, **265**, 440.
36.  Scwabe D., Sumathi R.R. 2005, , *J. Cryst. Growth*, **275**, e15.
37.  Suzuki T. 2004, *J. Cryst. Growth*, **270**, 511.

38.  Tokuhiro A., Takeda Y. 1993, *J. Cryst. Growth*, **130**, 421.
39.  Son S.-S., Yi K.W. 2005, *J. Cryst. Growth*, **275**, e249.
40.  Son S.-S., Yi K.W. 2005, *J. Cryst. Growth*, **275**, e259.
41.  Whiffin P.A.C., Bruton T.M., Brice J.C. 1976, *J. Cryst. Growth*, **32**, 205.
42.  Brandle C.D. 1977, *J. Cryst. Growth*, **42**, 400.
43.  Jones A.D.W. 1983, *J. Cryst. Growth*, **61**, 235.
44.  Jones A.D.W. 1983, *J. Cryst. Growth*, **63**, 70.
45.  Jones A.D.W. 1989, *J. Cryst. Growth*, **94**, 421.
46.  Tanaka M., Hasebe M., Saito N. 1997, *J. Cryst. Growth*, **180**, 487.
47.  Nakamura S., Eguchi M., Azami T., Hibiya T. 1999, *J. Cryst. Growth*, **207**, 55.
48.  Miyazawa Y. 1999, *Progr. Crystal Growth and Charact. Materials*, **38**, 261.
49.  Kishida Y., Okazawa K. 1999, *J. Cryst. Growth*, **198/199**, 135.
50.  Azami T., Nakamura S., Eguchi M., Hibiya T. 2001, *J. Cryst. Growth*, **233**, 99.
51.  Rappl P.H.O., Ferraz F.M., Scheel H.J., Barros M.R.X., Schiel D. 1984, *J. Cryst. Growth*, **70**, 49.
52.  Aleksic J., Szymczyk J.A. 2003, *PAMM*, **3**, 322.
53.  Kakimoto K., Eguchi M., Watanabe M., Hibiya T. 1989, *J. Cryst. Growth*, **94**, 412.
54.  Kakimoto K., Eguchi M., Watanabe M., Hibiya T. 1990, *J. Cryst. Growth*, **102**, 16.
55.  Kakimoto K., Watanabe M., Eguchi M., Hibiya T. 1992, *Int. J. Heat mass Transfer*, **35**, 2551.
56.  Watanabe M., Eguchi M., Kakimoto K., Baros Y., Hibiya T. 1993, *J. Cryst. Growth*, **128**, 288.
57.  Yi K.-W., Kakimoto K., Eguchi M., Watanabe M., Shyo T., Hibiya T. 1994, *J. Cryst. Growth*, **144**, 20.
58.  Kakimoto. K. 1995, *Appl. Phys. Rev.,* **77**, 1827.
59.  Kakimoto. K. 1995, *Progr. Crystal Growth and Charact. Materials*, **30**, 191.
60.  Watanabe M., Kakimoto K., Eguchi M., Hibiya T. 1997, *Jpn. J. Appl. Phys.,* **36**, 6181.
61.  Watanabe M., Yi K.W., Hibiya T., Kakimoto K., *1999. Progr. Crystal Growth and Crystallization of Materials*, **38**, 215.
62.  Imaishi N, Kakimoto K., 2002, *Ann. Rev. Heat Transfer*, **12,** 187.
63.  Gorbunov L., Klyukin A., Pedchenko A., Feodorov A., 2003, *Magnetohydrodynamics*, **39**, 521.
64.  Gorbunov L., Klyukin A., Pedchenko A., Feodorov A., 2003, *Energy Conversion and Management*, **43**, 317.
65.  Biberin V.I., Osvenskii V.B., Smirnov V.A., Starshinova I.V., Fryazinov V.I. 1985, *Sov. Phys. – Crystallography*, **30**, 568.
66.  Fontaine J.P., Randriamampianina A., Bontoux P. 1991. *Phys. Fluids A*, **3**, 2310.
67.  Anselmo A., Prasad V., Koziol G., Gupta K.P. 1993, *J. Cryst. Growth*, **134**, 116.
68.  Zhou W., Bornside D.E., Brown R.A. 1995, *J. Cryst. Growth*, **137**, 26.
69.  Sung H.J., Jung Y.J., Ozoe H. 1995, *Int J. Heat Mass Transfer*, **38**, 1627.
70.  Fontaine J.P., Bontoux P. Ouazzani J., Extrémet G.P., Raspo I., Chevrier V., Launay J.C. 1996, *Eur. J. Mech., B/Fluids*, **15**, 665.
71.  Okano Y., Audet N., Dost S., Hayakawa Y., Kumagawa M. 1998, *Int J. Numer. Model.,* **11**, 289.
72.  Rujano J.R., Crane R.A., Rahman M.M., Moreno W. 2002, *J. Cryst. Growth*, **245**, 149.

73.  Savolainen V., Heikonen J., Ruokolainen J., Anttila O., Laakso M., Paloheimo J. 2002, *J. Cryst. Growth*, **243**, 243.
74.  Banerjee J., Muralidhar K. 2006, *J. Cryst. Growth*, **286**, 350.
75.  Roy S., Roy A., Arora R.C. 2006, *Heat Mass Transfer*, **42**, 187.
76.  Mihelčić M., Wingerath K. 1989, *J. Cryst. Growth*, **97**, 42.
77.  Kakimoto K., Watanabe M., Eguchi M., Hibiya T. 1994, *J. Cryst. Growth*, **139**, 197.
78.  Xiao Q., Derby J.J. 1995, *J. Cryst. Growth*, **152**, 169.
79.  Givoli D., Flaherty J.E., Shephard M.S. 1997, *Int. J. Numer. Meth. Heat Fluid Flow*, **7**, 880.
80.  Akamatsu M., Kakimoto K., Ozoe H. 1997, *J. Mater. Proc. & Manufact. Sci.*, **5**, 329.
81.  Tomonari H., Iwamoto M., Kakimoto K., Ozoe H., Suzuki K., Fukuda T. 1998, *The Chem. Eng. J.*, **71**, 191.
82.  Kakimoto K., Ozoe H. 1998, *Comput. Mater. Sci.*, **10**, 127.
83.  Won Y.C., Kakimoto K., Ozoe H. 1999, *Numer. Heat Transfer, Pt. A*, **36**, 551.
84.  Rojo J.C., Derby J.J. 1999, *J. Cryst. Growth*, **198/199**, 154.
85.  Jing. C.J., Imaishi N., Yasuhiro S., Miyazawa Y., 1999. *J. Cryst. Growth*, **200**, 204.
86.  Jing. C.J., Imaishi N., Sato T., Miyazawa Y., 2000. *J. Cryst. Growth*, **216**, 372.
87.  Basu B., Enger S., Breuer M., Durst F. 2000, *J. Cryst. Growth*, **219**, 123.
88.  Enger S., Basu B., Breuer M., Durst F. 2000, *J. Cryst. Growth*, **219**, 144.
89.  Jing. C.J., Imaishi N., Yasuhiro S., Sato T., Miyazawa Y., 2000. *Int. J. Heat Mass Transfer*, **43**, 4347.
90.  Chatterjee A., Prasad V., Sun D. 2000, *Numer. Heat Transfer, Pt. A,* **37**, 823.
91.  Jing C.-J., Yasuhiro S., Suenaga H., Sato T., Imaishi N. 2000, *Thermal Sci. & Eng.,* **8**, 1.
92.  Wang W., Watanabe M., Hibiya T., Tanahashi T. 2000, *Jpn. J. Appl. Phys.*, **39**, 372.
93.  Vizman D., Friedrich J., Müller G. 2001, *J. Cryst. Growth*, 230, 73.
94.  Polezhaev V.I., Bessonov O.A., Nikitin N.V., Nikitin S.A. 2001, *J. Cryst. Growth*, **230**, 40.
95.  Enger S., Grabner O., Müller G., Breuer M., Durst F. 2001, *J. Cryst. Growth*, **230**, 135.
96.  Kohno H., Tanahashi T. 2001, *CMES*, **2**, 155.
97.  Vizman D., Gräbner O., Müller G. 2001, *J. Cryst. Growth*, **233**, 687.
98.  Won Y.C., Kakimoto K., Ozoe H. 2001, *J. Cryst. Growth*, **233**, 622.
99.  Basu B., Enger S., Breuer M., Durst F. 2001, *J. Cryst. Growth*, **230**, 148.
100. Kohno H., Tanahashi T. 2002, *J. Comput. Appl. Math.*, **149**, 359.
101. Ivanov N.G., Smirnov E.M. 2002, *J. Eng. Phys. And Themophys.*, **75**, 599.
102. Vizman D., Gräbner O., Müller G. 2002, *J. Cryst. Growth*, **236**, 545.
103. Kakimoto K., Tashiro A., Shinozaki T., Ishii H., Hashimoto Y. 2002, *J. Cryst. Growth*, **243**, 55.
104. Kumar V., Biswas G., Brenner G., Durst F. 2003, *Int. J. Heat mass Transfer*, **46**, 1641.
105. Zeng Z., Chen G., Mizuseki H., Shimamura K., Fukuda T., Kawazoe Y. 2003, *J. Cryst. Growth*, **252**, 538.
106. Jing C.J., Kobayashi M., Tsukada T., Hozawa M., Fukuda T., Imaishi N., Shimamura K., Ichinose N. 2003, *J. Cryst. Growth*, **252**, 550.
107. Kumar V., Basu B., Enger S., Brenner G., Durst F. 2003, *J. Cryst. Growth*, **255**, 27.
108. Bänsch E., Davis D., Langmach H., Miller W., Rehsa U., Reinhardt G., Uhle M. 2004, *J. Cryst. Growth*, **266**, 60.

109. Zhao G.J., Zeng X.H., Zhou S.M., Xu J., Tian Y.L., Huang W.X. 2003, *Phys. Stat. Sol (a)*, **199**, 186.
110. Li Y.R., Imaishi N., Peng L., Wu S.-Y., Hibiya T. 2004, *J. Cryst. Growth*, **266**, 88.
111. Zheng Z., Chen J., Mizuseki H., Fukuda T., Kawazoe Y. 2004, *J. Cryst. Growth*, **266**, 81-87.
112. Kitashima T., Liu L., Kitamura K., Kakimoto K. 2004, *J. Cryst. Growth*, **267**, 574.
113. Zeng Z., Chen J., Mizuseki H., Sato H., Shimamura K., Ichinoseki K., Fukuda T., Kawazoe Y. 2004, *Mater. Trans.*, **45**, 1515.
114. Schäfer F., Kumar V., Breuer M., Durst F. 2005, *Int. J. Comput. Fluid Dyn.,* **19**, 501.
115. Liu L., Kakimoto K. 2005, *Int. J. Heat Mass Transfer*, **48**, 4481.
116. Liu L., Kakimoto K. 2005, *Int. J. Heat Mass Transfer*, **48**, 4492.
117. Liu L., Kakimoto K. 2005, *Cryst. Res. Technol*., **40**, 347.
118. Li Y.-R., Quan X.-J., Peng L., Imaishi N., Wu S.-Y., Zeng D.-L. 2005, *Int. J. Heat Mass Transfer*, **48**, 1952.
119. Tsukada T., Kobayashi M., Jing C.J., and Imaishi N. 2005, *Fluid Dynamics and Material Processing*, **1**, 45.
120. Bänsch E., Davis D., Langmach H., Reinhardt G., Uhle M. 2006, *Computers and Fluids*, **35**, 1400.
121. Nikitin N., Polezhaev V. 1999, *Fluid Dynamics*, **34**, 322.
122. Nikitin N., Polezhaev V. 2001, *J. Cryst. Growth*, **230**, 30.
123. Walker J.S., Henry D., Ben Hadid H. 2002, *J. Cryst. Growth*, **243**, 108.
124. Gelfgat A.Yu., Rubinov A., Bar-Yoseph P.Z., Solan A. 2005, *J. Cryst. Growth*, **275**, e7.
125. Gelfgat A.Yu*. 2007, Int. J. Numer. Meths. Fluids*, **53**, 485.
126. Gelfgat A.Yu. 2007, *Int. J. Numer. Meths. Fluids*, **54**, 269.
127. Gelfgat A.Yu., Rubinov A., Bar-Yoseph P.Z., Solan A. 2005, *Fluid Dynamics and Material Processing*, **1**, 21.